Infrared Spectrum of the Palladium Nitrosyl Complex Isolated in Solid Argon

Lahouari Krim, Esmaïl M. Alikhani, and Laurent Manceron*

LADIR/Spectrochimie Moléculaire, UMR 7075 CNRS, Université Pierre et Marie Curie, Boîte 49, 4 Place Jussieu, 75252 Paris, Cedex 05, France

Received: March 27, 2001; In Final Form: June 5, 2001

The reaction of ground-state Pd atoms with NO during condensation in solid argon has been reinvestigated. The Pd(η^1-NO) molecule, already characterized in reactions of laser-ablated Pd, is the only product observed for the reaction between one Pd atom and one nitric oxide molecule. Isotopic data on ν_1, ν_2, and ν_3 have been measured in the mid- and far-infrared regions. These enable an independent estimate of the molecular shape on the basis of complete harmonic force-field calculations. The molecule is bent, with a Pd−N−O bond angle around 115 ± 15°, in basic agreement with theoretical predictions. This study provides a useful test for comparing the performance of various quantum mechanical methods for reproducing the spectroscopic properties. The bonding in Pd- and NiNO is analyzed using natural bonding orbital and topological methods.

Introduction

The wide interest in modeling the chemisorption or chemical interaction of small absorbates such as NO or CO on metal surfaces or supported metal-containing species has motivated both theoretical and experimental studies on related "model" systems such as the interaction of an isolated metal atom with one ligand molecule.[1−11] In particular, the interaction of Pd atoms with NO has been the object of recent theoretical studies using either generalized valence bond and configuration interaction (GVB−CI) methods[12] or density functional (DF) calculations.[13] The motivation for these works is to provide results on well-defined, small-size systems before extending the methodology to larger clusters or to periodic surfaces.[14] Obviously, reliable experimental data on the very same species are also needed, and a recent study has provided the first elements of comparison, isolating $PdNO^+$, PdNO, and $PdNO^-$ species among the reaction products of laser-ablated palladium atoms with NO molecules.[15] This study provided the first identification of these species through the observation of nitrosyl stretching vibrations and compared these observations with the predictions of other DF calculations. IR bands consistent with the two other stretching or bending modes of PdNO were not detected. It seems, however, that this information also constitutes testing grounds of the quality of the many theoretical studies attempting to describe the Pd−NO bonding. These are sensitive markers for the quality of the metal−ligand interaction description as the associated normal coordinate follows more closely the reaction coordinate.

Recently we have shown that it is possible to obtain complete sets of vibrational data for the MCO and MNO triatomics and derive M−C and M−N force constants, which are directly related to the strength of the coordination.[16−19] In this study we present an investigation in the far-infrared range of the low-frequency stretching and bending modes of PdNO isolated in solid argon, to bring additional information on the structure of the PdNO triatomic molecule. We have used the thermal evaporation technique which enables one to scale-up the production of the neutral species and report here the frequencies of the Pd−NO stretching and bending vibrations, ν_1, ν_3, and ν_2, for several isotopic species ($^{14}N^{16}O$, $^{15}N^{16}O$, and $^{14}N^{18}O$ isotopic species for NO).

Experimental Section

The Pd + NO species were prepared by co-condensing Pd vapor and NO/Ar mixtures (0.1−4% molar ratios) onto a cryogenic metal mirror maintained around 10 K. The experimental methods and setup have been previously described.[17] Briefly, here, a tungsten filament, mounted in a furnace assembly and wrapped with palladium wire (Alpha Inorganics, 99.9%), was heated resistively from 1200 to 1400 °C to generate the Pd vapor. Metal deposition rates, monitored with a microbalance, were typically of the order of 0.10−0.80 μg/min. Deposition times were around 120 min.

Argon gas ("L'Air liquide", St. Quentin, France, 99.995% purity) was used without purification. NO ("L'Air Liquide" with a stated chemical purity of 99.9%) and ^{15}NO gas ("Isotec", Miamisburg, with a stated isotopic purity of 97.8%) were passed above mercury and further purified by vacuum trap-to-trap distillations before each experiment to eliminate slow N_2, N_2O, and NO_2 impurity buildup. $^{14}N^{18}O$ was prepared in the laboratory by addition of $^{18}O_2$ onto $^{14}N^{16}O$ gas to form $^{14}N^{(16+18)}O_2$ which was subsequently reduced to $^{14}N^{18}O$ and $^{14}N^{16}O$ by reaction with mercury.[20] The resulting gas is a mixture containing approximately 52% $^{14}N^{16}O$ and 48% $^{14}N^{18}O$ and was also purified using trap-to-trap vacuum distillations. The sample purity was confirmed spectroscopically.

In general, after 2 h of deposition time, infrared spectra of the resulting sample were recorded in the transmission-reflection mode between 5000 and 70 cm^{-1} using a Bruker 120 FTIR spectrometer and suitable combinations of CaF_2/Si, KBr/Ge, or 6 μm Mylar beam splitters with either liquid N_2-cooled InSb or narrow-band HgCdTe photodiodes or a liquid He-cooled Si−B bolometer, fitted with cooled band-pass filters. Also, absorption spectra in the near-, mid-, and far-infrared were collected on the *same* samples through either CaF_2, CsI, or polyethylene windows mounted on a rotatable flange separating the interferometer vacuum (10^{-2} mbar) from that of the cryostatic cell (10^{-7} mbar). The resolution was varied between 0.1 and 0.5 cm^{-1}. Bare mirror backgrounds, recorded at 10 K from 5000 to 70 cm^{-1} prior to sample deposition, were used as

10.1021/jp0111416 CCC: $20.00
Published on Web 07/31/2001

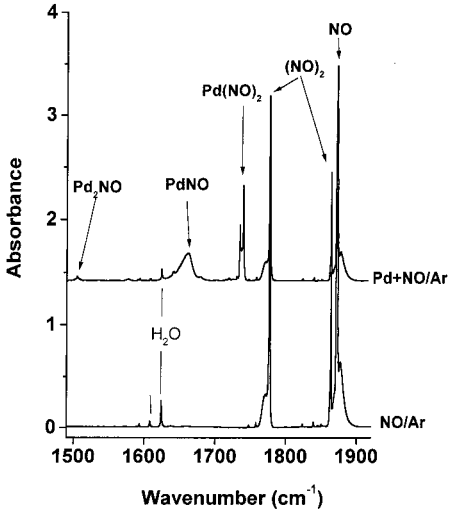

Figure 1. Infrared spectrum in the 1900−1500 cm^{-1} nitrosyl stretching region for (a) Pd/NO/Ar = 0.5/1/100 sample and (b) the same without metal.

references in processing the sample spectra. The spectra were subsequently subjected to baseline correction to compensate for infrared light scattering and interference patterns.

Results

In samples where Pd atoms were co-deposited with relatively dilute NO/Ar mixtures, infrared spectra in the metal nitrosyl N−O stretching region (1300−1900 cm^{-1}) presented four absorptions in addition to those attributed to unreacted NO, $(NO)_2$, and their isotopomers (Figure 1). These absorptions can be detected even in diluted samples near 1740, 1661, 1504 and 1516 cm^{-1}. After study of the variation of these signals over a wide Pd or NO concentration range, it appears that they present either linear or quadratic dependences. The two lower bands, observed at 1516.0 and 1504.4 cm^{-1}, present a second-order dependence with respect to the metal atom concentration and a first-order dependence with respect to the NO concentration. The main band at 1504 cm^{-1} has been previously assigned to a Pd_2NO species in the recent laser ablation study,[15] in agreement with the present results. In the thermal evaporation experiments a second, slightly different argon matrix trapping site seems responsible for the minor 1516 cm^{-1} absorption. The broad band near 1661 cm^{-1} (fwhm = 19 cm^{-1}) has a linear concentration dependence in either reagent and, thus, corresponds to a molecular species containing one Pd atom and one NO molecule, in agreement with the conclusions of Citra and Andrews PdNO.[15] Finally the multiplet detected around 1740 cm^{-1} presents first- and second-order dependences in Pd and NO, respectively, consistent with the conclusions of Citra and Andrews, who assigned this signals to $Pd(NO)_2$ species trapped in multiple sites in the argon matrix. New information relative to this species will be discussed in the following paper.

We will focus here on the palladium mononitrosyl species. Samples obtained with varying concentrations of NO and Pd in argon matrix present two bands, located at 522.1 and 229.8 cm^{-1}, whose relative intensities remain constant with respect to the 1661.3 cm^{-1} band. Typically all these bands increased after slightly annealing the matrix from 10 to 20 K but remained constant after a more marked annealing up to 35 K, which favors the larger aggregates such as $Pd(NO)_2$. Each of these bands appears as a doublet in spectra obtained with NO isotopic mixtures ($^{14}N^{16}O/^{15}N^{16}O$ or $^{14}N^{16}O/^{14}N^{18}O$; see Figure 2) and is therefore attributed to the same molecule, PdNO. UV light

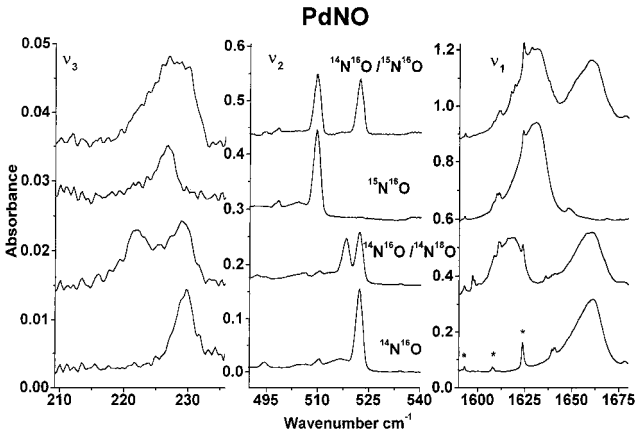

Figure 2. Infrared spectrum in the ν_1, ν_2, and ν_3 region of PdNO: (a) $Pd/^{14}N^{16}O/Ar = 0.5/1/100$; (b) same with $^{14}N^{16}O/^{14}N^{18}O = 0.6/0.4$; (c) same with $^{15}N^{16}O$; (d) same with $^{14}N^{16}O + {}^{15}N^{16}O = 0.55/0.45$.The asterisks designate water impurity lines.

TABLE 1: Observed Frequencies (in cm^{-1}) for the $Pd^{14}N^{16}O$, $Pd^{15}N^{16}O$, and $Pd^{14}N^{18}O$ Isotopic Species of Palladium Mononitrosyl Isolated in an Argon Matrix (Relative Intensities with Respect to the Strongest Fundamental in Parentheses)

assgnt	$Pd^{14}N^{16}O$	$Pd^{15}N^{16}O$	$Pd^{14}N^{18}O$
ν_3	229.8 (0.0014)	226.8	222.0
ν_2	522.1, 510.3 (0.035)	509.6, 498.2	518.0, 506.6
ν_1	1661.3 (1)	1630.7	1617.6

irradiation at 313 nm causes these three absorptions to decrease significantly in intensity but does not affect the dinitrosyl bands. In addition to helping in correlating these three absorptions, this indicates the existence of a dissociative excited state some 4 eV above the ground state for this species. The absorptions observed for the different isotopic species of PdNO are listed in Table 1. The broad band near 1661 cm^{-1} experiences a relatively large shift with ^{18}O substitution and a smaller one with ^{15}N, to 1617.6 and 1630.7 cm^{-1}, respectively (Figure 2). The low-frequency absorptions also appear with asymmetrical profiles, but all bands remained unresolved even using 0.1 cm^{-1} resolution. For the band at 522.1 cm^{-1} shifting to 509.6 and 518.0 cm^{-1} upon replacing $^{14}N^{16}O$ by $^{15}N^{16}O$ and $^{14}N^{18}O$, respectively, a weaker signal near 510 cm^{-1} follows a parallel evolution with either concentration, temperature, and isotopic effects and is therefore attributed to a site effect (the other bands near 1661 and 230 cm^{-1} are notably broader and show either asymmetric profiles or shoulders which are likely due to inhomogeneous broadening). The band at 229.8 cm^{-1} is shifted to 226.8 and 222.0 cm^{-1} (Figure 2), with these same precursors.

Discussion and Vibrational Analysis. Three bands pertaining to PdNO have been measured at 1661.3, 522.1, and 229.8 cm^{-1}. Among these absorptions the 1661.3 cm^{-1} band has been formerly assigned to the NO stretching vibration of PdNO, ν_1. This band shifts to lower frequency by 30.6 cm^{-1} when $^{15}N^{16}O$ is used and by 43.7 cm^{-1} with $^{14}N^{18}O$; the ν_1 frequency for $Pd^{15}N^{16}O$ is thus larger than that for $Pd^{14}N^{18}O$. There is very little difference between the $^{14}N/^{15}N$ and $^{16}O/^{18}O$ effects for the palladium nitrosyl complex (1630.7 − 1617.6 = 13.1 cm^{-1}) and those for an isolated NO harmonic oscillator at the same frequency (1631.2 − 1617.4 = 13.8 cm^{-1}, which is practically the value for the NO diatomics 1839.0 − 1823.4 = 15.6 cm^{-1}, when scaled down to the frequency range). In the related NiNO ($^2A'$) species, which presented stretching frequency in this region (1677 cm^{-1}), this difference was only 1643.9 − 1640.9 = 3 cm^{-1}. This indicates a much reduced coupling between the

TABLE 2: Comparison of Observed for $Pd^{14}N^{16}O$ Isolated in Solid Argon and Calculated Harmonic Frequencies (cm^{-1}) by Various Quantum Mechanical Methods

assgnt	obsd	GVB/PP[a]	BPW91[b] LanL2DZ/6-311+ G(d)	BP3LYP[c] LanL2DZ/6-311+G (d)	BP3LYP[d] SDD/6-311+G(2d)
ν_3 bending mode	229.8 (0.14)[e]	292.0	257 (4)[f]	228 (4)	235 (4)
ν_2 Pd−N stretching mode	522.1 (3.5)	671.0	534 (6)	480 (7)	496 (7)
ν_1 NO stretching mode	1661.3 (100.0)	1686.0	1700 (750)	1787 (730)	1762 (754)

[a] The geometric parameters of the PdNO are $r_{NO} = 1.17$ Å, $r_{PdN} = 1.9$ Å, and ∠PdNO = 113°.[12] [b] $r_{NO} = 1.18$ Å, $r_{PdN} = 1.89$ Å, and ∠PdNO = 127°.[15] [c] $r_{NO} = 1.167$ Å, $r_{PdN} = 1.93$ Å, and ∠PdNO = 128°.[15] [d] $r_{NO} = 1.166$ Å, $r_{PdN} = 1.904$ Å, and ∠PdNO = 127° (this work). [e] Relative IR intensities with respect to the most intense mode. [f] Absolute IR intensities in km/mol.

M−NO and N═O coordinates in PdNO compared to NiNO. This can be due to a decrease in the M−N═O bond angle or in the M−N bond force constant or a combination of both effects, as discussed below.

The 522.1 cm^{-1} band shifts to lower frequency by 12.5 cm^{-1} when $^{14}N^{16}O$ is substituted by $^{15}N^{16}O$, while substitution of $^{14}N^{16}O$ by $^{14}N^{18}O$ causes a smaller shift, about 4.1 cm^{-1}. Conversely, the lower frequency mode shows a smaller shift with $^{15}N^{16}O$ than with $^{14}N^{18}O$ (3.0 vs 7.8 cm^{-1}). The 522.1 cm^{-1} band is about 25 times more intense than the lower frequency band and cannot be attributed to a binary level. These two absorptions are thus due to two different fundamentals, the remaining metal−nitrosyl bending and stretching vibrations.

The results of the most recent theoretical studies, which have calculated the three frequencies for PdNO in the $^2A'$ ground state, are given in Table 2. Comparisons of observed vibrational transitions for the matrix-isolated molecules and ab initio harmonic frequencies should be made with the usual caution. Due to matrix perturbations on one hand and neglect of anharmonicity on the other we will thus limit comparison to general trends. Obviously, the GVB calculation overestimates the metal−ligand vibrations. For instance, the intermediate energy vibration, mainly describe as a Pd−NO stretching, is 28% too high, which is surprising in view of the calculated small binding energy ($D_e \approx 4$ kcal/mol). The more recent DF calculations did not state the calculated binding energies, but only the energy separation with the first excited state, the lowest quartet state, calculated much higher. The frequencies calculated in ref 15 for the $^2A'$ ground state are in much better overall agreement with the observed frequencies (18, 5.5, and 5% standard deviations for the GVB, BPW, and B3LYP, respectively). Contrary to statements based only on the ligand upper frequency stretching ν_1 mode, the B3LYP frequencies are not specifically overestimated. When all results are considered, the low-frequency modes are slightly underestimated, especially considering the neglect of anharmonic effects. Characteristically, the deviations with experimental frequencies vary relatively little from method to method when considering the ν_1 mode (1−7%), compared to the low-frequency metal−ligand vibrations (28−4% average deviations). Calculations made here using the same DF method[21,22] but slightly augmented basis sets (6-311+G(2d))[23] and the Stuttgart pseudopotential[24] yielded only very slightly better results for frequencies (Table 2) and predict a binding energy around 30 kcal/mol with respect to the separate fragments.

Semiempirical harmonic force field calculations were performed to test the information about the predicted bonding properties and molecular shape of the PdNO molecule. First, on the basis of the equilibrium geometry calculated with in ref 12 ($r_{NO} = 1.17$ Å, $r_{PdN} = 1.90$ Å, and ∠PdNO = 113°), we searched the set of potential constants which yielded an acceptable agreement with the experimental results. Next, to test the geometry, we varied the PdNO bond angle stepwise between 180 and 80° (the bond lengths are thus kept constant).

TABLE 3: Observed and Calculated[a] Frequencies (cm^{-1}) of the Various Isotopic Species of PdNO[b] ($^2A'$) Using a Semiempirical Harmonic Force Field

$Pd^{14}N^{16}O$		$Pd^{15}N^{16}O$		$Pd^{14}N^{18}O$		
obsd	calcd	obsd	calcd	obsd	calcd	assgnt
229.8	229.6	226.8	226.8	222.0	221.8	ν_3
522.1	522.1	509.6	510.0	518.0	517.5	ν_2
1661.3	1661.3	1630.7	1631.0	1617.6	1618.5	ν_1

[a] The force constants are $F_{NO} = 12.2$ mdyn Å^{-1}, $F_{PdN} = 3.15$ mdyn Å^{-1}, $F_{PdNO} = 0.5$ mdyn Å rad^{-2}, $F_{NO,PdNO} = 0.8$ mdyn rad^{-1}, and $F_{PdN,PdNO} = 0.78$ mdyn rad^{-1}. [b] The geometric parameters of PdNO are $r_{NO} = 1.17$ Å, $r_{PdN} = 1.9$ Å, and ∠PdNO = 115°.

For each given angle, the best set of potential constant is searched for, on the basis of the overall agreement with the experimental isotopic shifts ($^{14}N^{16}O/^{15}N^{16}O$ and $^{14}N^{16}O/^{14}N^{18}O$) on all three ν_1, ν_2, and ν_3 modes. The best results (Table 3) are obtained for a bond angle in the vicinity of that calculated by all quantum chemical methods (∠PdNO = 115 ± 15°), with the error bars indicated here coming from the experimental uncertainties on the isotopic shifts. These considerations are based on crude harmonic oscillator models known to estimate structural parameters deviating by a few degrees from known values,[25] but the trends should be meaningful when comparing, for instance, the nitrosyl PdNO (≈115°) and NiNO (≈136°) bond angle values. The normal coordinate description at this level indicates that the lowest frequency mode, ν_3, implies mainly the bending coordinate, and ν_2, the Pd−NO stretching. The predicted Pd isotope effects are largest on this mode, but represents about 0.4 cm^{-1} per mass unit, which is well within the homogeneous bandwidth, at the difference of the linear palladium carbonyl triatomics.[17] The N−O, Pd−N, and Pd−N−O force constants are of the order of 12.2 mdyn Å^{-1}, 3.15 mdyn Å^{-1}, and 0.5 mdyn Å rad^{-2}, respectively. It should be noticed that for both NiNO and PdNO molecule, the NO force constants remain close (F_{NO} =11.4 and 12.2 mdyn Å^{-1} , in NiNO and PdNO, respectively), while the metal−N force constant is about 1.4 times larger in NiNO. Also, in contrast to NiNO, a second isomeric form with a side-on cyclic structure is not observed for PdNO.

Electronic Structure and Bonding. Two questions are of interest to discuss the specificity of palladium in the formation of mononitrosyl complexes: first, the absence of a metastable side-bonded form is notable, and second, the reason for the bent molecular shape (in contrast to the dinitrosyl species discussed in the following paper).

Concerning the first point, the Pd + NO potential surface was explored systematically at the B3LYP level,[21,22] using the 6-311+G(2d)[23] for N and O atoms and the 18-valence electron Stuttgart pseudopotential[24] for Pd. All calculations have been performed with the Gaussian 98/DFT quantum chemical package.[26] Any attempt at optimization starting from a geometry with comparable Pd−N and Pd−O distances resulted in an opening of the Pd−N═O bond angle, so no metastable

TABLE 4: Topological ELF Population Analysis (in e)

compds	V(O)[a]	V(N)[a]	V(N, O)[b]	V((N, M)[b]/M[c])	V((O, M)[b]/M[c])	V(M)[a]	C(M)[d]
NO	4.78	3.80	2.17				
Ni(η^1-NO)	5.26	2.94	1.71	1.52/0.66		0.36	26.98
Ni(η^2-NO)	2.95	2.18	1.54	2.3/0.16	2.54/0.09	0.63	27.1
Pd(η^1-NO)	5.15	2.38	1.84	1.78/0.36			45.7

[a] Monosynaptic basin. [b] Disynaptic basin. [c] M = Ni, Pd metal atom contribution. [d] Core basin.

minimum could be found. Fixed point calculations also show that any side-on or pseudocyclic configuration yield a total energy above that of the separate fragments, at the difference of the Ni + NO system. This result is in agreement with the absence of any η^2-NO monometallic species in our experiments.

With palladium, the atomic singlet ground state with the empty 5s shell certainly favors the end-on coordination. The bending of the molecular frame in the Ni−NO case could have been due to repulsion between the Ni 4s−3d hybrid and NO 5σ electrons antibonding HOMO.[9] With palladium, the higher energy of the 5s shell could weaken this consideration, and one would intuitively think that 4d−π* interaction should be the driving force and thus expect a linear $^2\Pi$ configuration. This bring us to the second point: the reason behind the nonlinearity of the molecule. Constraining a Pd−NO linear approach leads to a $^2\Pi$ bound state ($D_e \approx 23$ kcal/mol below the separate fragments) but with an imaginary frequency for the bending mode. This can be readily understood given that a $^2\Pi$ configuration for a triatomics corresponds to a first-order Renner−Teller situation, where bending of the molecular frame will lift the degeneracy of the Π* SOMO pair. Allowing all degrees of freedom to relax at this point results in a splitting of the formerly degenerate $^2\Pi$ state into ^{2}A′ and ^{2}A″ configurations in which the SOMO corresponds to the in- or out-of plane molecular orbital. The calculation shows a sizable stabilization (−6 kcal/mol) of the ^{2}A′ configuration which now has three real frequencies (the energy of the other state can be roughly estimated by exciting one β electron and also shows a small stabilization). So both the magnitude of the stabilization upon bending and the similarity in structure for NiNO despite a Ni $3d^8\ 4s^2$ or $3d^9\ 4s^1$ atomic configuration point to another direction, inherent to the metal−NO bonding mechanism. In addition to the calculations of energetic, structural, and vibrational properties of PdNO we have attempted to analyze the metal−nitrosyl bonding either in the molecular orbital picture or in the global topological approach.

First, to describe the bonding in the traditional terms of σ-donation/π-back-donation picture, we have investigated the orbital rehybridization using the natural bonding orbital (NBO) method.[27] Taking the molecule in the *xy* plane with the Pd−N bond along the *y* axis, we have the Pd $4d_{xy}$, $4d_{x^2-y^2}$, 5s as well as the former NO 5σ and π* MOs, all with with symmetry A′. On the other hand, the $4d_{xz}$ and $4d_{yz}$ and the empty π* MO have A″ symmetry. Clearly the metal to ligand charge transfer originates from the stabilizing interaction between the empty NO π* MO and the filled $4d_{yz}$ of palladium, but this interaction is not qualitatively affected by the bending of the molecular frame. What is critical in the latter effect is that two important rehybridizations can then take place: first, the empty 5s can combine with the $4d_{x^2-y^2}$, to form two possible hybrids denoted a′ and a′*, respectively, filled and empty. Also for NO, the $\sigma-\pi$ separation no longer holds and two new MOs appear to be mostly localized around the nitrogen atom. One is filled and can be very approximately described as a 2s and $2p_x$ hybrid, and the other, semifilled, as a 2s and $2p_y$ hybrid which overlap favorably with the metal a′* hybrid to form the semifilled covalent σ bonding orbital along the Pd−N axis. Bending the molecular frame is crucial for this interaction to take place, and we believe that this mechanism is also responsible for the bent shape of the isoelectronic $PdCO^-$ anion.[28]

Although the usual picture of σ donation/π back-donation by means of natural orbital provides a qualitative description of the metal−ligand bonding, it is only the total electron distribution obtained by summing electron densities overall the orbitals of the molecular space that has real physical significance. To complete our understanding we have also studied the system using the electron localization function (ELF)[29] and the atoms in molecules topological methods.[30] In principle, the topological analysis using ELF should be restricted to all-electrons wave functions. Recently, Silvi et al. showed that, with small core pseudopotentials, the external part of the core gives rise to well-defined basins which share boundaries with the surrounding basins; therefore, the analysis can be carried out safely,[31] even in this restricted framework. Here, the topological data combining the ELF/AIM approaches have been obtained with a small core potential for the metal. All topological calculations have been carried out using the Top-Mod package.[32] In the ELF approach, the molecular space is partitioned into basins of attractors having clear chemical signification. These are either core basins surrounding nuclei or valence basins. The valence basins are characterized by their synaptic order which is defined as the number of core basins with which they share a common boundary. Accordingly, monosynaptic basins correspond to lone pair regions (designated as V(X) where X denotes atom labels) and disynaptic ones correspond to bonding regions (V(X, Y) shared by atom X and Y). A complete description can be found in ref 32. In the AIM topology, nuclei are attractors of the electron density (ρ) gradient vector field. The molecular space is disjointly partitioned into basins (where $\nabla\rho = 0$), and an atom in a molecule is thus defined as the union of an attractor and its basin. From the ELF approach and the metal atomic basin from the AIM topology, one can calculate the valence basin population between the metal atom and the coordinated atom of the ligand unit (denoted as V(L, M), where L = N, O and M = Ni, Pt). It is then possible to determine the metal contribution in the bonding region by calculating the intersection of the two basins. This contribution is labeled as V((L, M)/M). For instance, the valence basin between the nickel and nitrogen atoms in the Ni(η^1-NO) complex is given by V((N, Ni)/Ni) = 1.52/0.66, where 1.52 e is the population of this disynaptic basin and 0.66 e the Ni participation in this basin. The results for NO, both isomeric forms of NiNO (η^1-NO and η^2-NO), and PdNO are presented in Table 4. These results reflect the strong decrease in the V(N,O) disynaptic basin going from Ni(η^1-NO) to the other tautomeric form of NiNO, compared to the reverse effect, when switching to PdNO. Also, the metal participation in the metal−ligand disynaptic basin is reduced from 1.52/0.66 for Ni−NO, compared to 1.78/0.36 in Pd−NO, which should be paralleled to the decrease in binding energies (43 vs 30 kcal/mol) and in M−N force constants. The population of the nitrogen atom lone pair basin, responsible for the bent shape of both molecules, remains however relatively constant.

References and Notes

(1) Bauschlicher, C. W.; Bagus, P. S. *J. Chem. Phys.* **1984**, *80*, 944.
(2) Bagus, P. S.; Hermann, K.; Bauschlicher, C. W., Jr. *J. Chem. Phys.* **1984**, *80*, 4378.
(3) Fournier, R. *J. Chem. Phys*. **1993**, *99*, 1801.
(4) Persson, B. J.; Roos, B. O.; Pierloot, K. *J. Chem. Phys*. **1994**, *101*, 6810.
(5) Bauschlicher, C. W. *J. Chem. Phys*. **1994**, *100*, 1215.
(6) Schwerdtfeger, P.; Bowmaker, G. A. *J. Chem. Phys*. **1994**, *100*, 4487.
(7) Bauschlicher, C. W. *Chem. Phys. Lett*. **1994**, *229*, 577.
(8) Adamo, C.; Lelj, F. *J. Chem. Phys*. **1995**, *103*, 10605.
(9) Blanchet, C.; Duarte, H.; Salahub, D. R. *J. Chem. Phys.* **1997**, *106*, 8778.
(10) Darling, J. H.; Ogden, J. S. *J. Chem. Soc., Dalton Trans.* **1972**, 2496.
(11) Zhou, M.; Andrews, L. *J. Phys. Chem. A* **2000**, *104*, 3915.
(12) Smith, G. W.; Carter, E. A. *J. Phys. Chem.* **1991**, *95*, 2327.
(13) Rochefort, A.; Fournier, R. *J. Phys. Chem*. **1996**, *100*, 13506.
(14) Loffreda, D.; Simon, D. Sautet, P. *Chem. Phys. Lett*. **1998**, *291*, 15.
(15) Citra, A.; Andrews, L. *J. Phys. Chem. A* **2000**, *104*, 8160.
(16) Joly, H. A.; Manceron, L. *Chem. Phys.* **1998**, *226*, 61.
(17) Tremblay, B.; Manceron, L. *Chem. Phys*. **1999**, *250*, 187.
(18) Manceron, L.; Alikhani, M. E.; Tremblay, B. *J. Phys. Chem. A* **2000**, *104*, 3750.
(19) Krim, L.; Manceron, L.; Alikhani, M. E. *J. Phys. Chem. A* **1999**, *103*, 2598.
(20) Clusius, K. *Angew. Chem*. **1954**, *66*, 497.
(21) Becke, A. D. *J. Chem. Phys.* **1993**, *98*, 5648.
(22) Lee, C.; Yang, W.; Parr, R. G. *Phys. Rev. B* **1988**, *37*, 785.
(23) Frisch, M. J.; Pople, J. A.; Binkley, J. S. *J. Chem. Phys.* **1984**, *80*, 3265.
(24) Andrae, D.; Haeussermann, U.; Dolg, M.; Stoll, H.; Preuss, H. *Theor. Chim. Acta* **1990**, *77*, 123.
(25) Green, D.; Ervin, K. M. *J. Mol. Spectrosc*. **1981**, *88*, 51.
(26) Frisch, M. J.; Trucks, G. W.; Schlegel, H. B.; Gill, P. M. W.; Johnson, B. G.; Robb, M. A.; Cheeseman, J. R.; Keith, T.; Petersson, G. A.; Montgomery, J. A.; Raghavachari, K.; Al-laham, M. A.; Zakrzewski, V. G.; Ortiz, J. V.; Foresman, J. B.; Cioslowski, J.; Stefanov, B. B.; Nanayakkara, A.; Challacombe, M.; Peng, C. Y.; Ayala, P. Y.; Chen, W.; Wong, M. W.; Andres, J. L.; Replogle, E. S.; Gomperts, R.; Martin, R. L.; Fox, D. J.; Binkley, J. S.; Defrees, D. J.; Baker, J.; Stewart, J. P.; Head-Gordon, M.; Gonzalez, C.; Pople J. A. *Gaussian 98 (Revision A.7)*; Gaussian, Inc.: Pittsburgh, PA, 1998.
(27) Reed, A. E.; Curtiss, L. A.; Weinhold, F. *Chem. Rev.* **1988**, *80*, 899.
(28) Liang, B.; Zhou, M.; Andrews, L. *J. Phys. Chem. A* **2000**, *104*, 3905.
(29) Silvi, B.; Savin, A. *Nature* **1994**, *371*, 683.
(30) Bader, R. F. W. *Atom in Molecules: A Quantum Theory*; Oxford University Press: Oxford, U.K., 1994.
(31) Joubert, L.; Silvi, B.; Picard, G. *Theor. Chem. Acc*. **2000**, *104*, 109.
(32) Noury, S.; Krokidis, X.; Fuster, F.; Silvi, B. *Comput. Chem.* **1999**, *23*, 597.